Journal of Biomedical Optics

SPIEDigitalLibrary.org/jbo

Classification of inflammatory bowel diseases by means of Raman spectroscopic imaging of epithelium cells

Christiane Bielecki
Thomas W. Bocklitz
Michael Schmitt
Christoph Krafft
Claudio Marquardt
Akram Gharbi
Thomas Knösel
Andreas Stallmach
Juergen Popp

SPIE

Classification of inflammatory bowel diseases by means of Raman spectroscopic imaging of epithelium cells

Christiane Bielecki,[a*] Thomas W. Bocklitz,[b*] Michael Schmitt,[b] Christoph Krafft,[c] Claudio Marquardt,[a] Akram Gharbi,[d] Thomas Knösel,[e] Andreas Stallmach,[a*] and Juergen Popp[b,c*]
[a]University Hospital Jena, Department of Internal Medicine II, Division of Gastroenterology, Hepatology, and Infectious Diseases, Jena, Germany
[b]Friedrich-Schiller-University, Institute of Physical Chemistry and Abbe Center of Photonics, Jena, Germany
[c]Institute of Photonic Technology, Albert Einstein Straße 9, Jena, Germany
[d]University Hospital Jena, Clinic for General, Visceral and Vascular Surgery, Jena, Germany
[e]University Hospital Jena, Institute of Pathology, Jena, Germany

Abstract. We report on a Raman microspectroscopic characterization of the inflammatory bowel diseases (IBD) Crohn's disease (CD) and ulcerative colitis (UC). Therefore, Raman maps of human colon tissue sections were analyzed by utilizing innovative chemometric approaches. First, support vector machines were applied to highlight the tissue morphology (=Raman spectroscopic histopathology). In a second step, the biochemical tissue composition has been studied by analyzing the epithelium Raman spectra of sections of healthy control subjects ($n = 11$), subjects with CD ($n = 14$), and subjects with UC ($n = 13$). These three groups exhibit significantly different molecular specific Raman signatures, allowing establishment of a classifier (support-vector-machine). By utilizing this classifier it was possible to separate between healthy control patients, patients with CD, and patients with UC with an accuracy of 98.90%. The automatic design of both classification steps (visualization of the tissue morphology and molecular classification of IBD) paves the way for an objective clinical diagnosis of IBD by means of Raman spectroscopy in combination with chemometric approaches. [DOI: 10.1117/1.JBO.17.7.076030]

Keywords: biophotonics; image analysis; medicine; Raman spectroscopy.

Paper 12204 received Mar. 29, 2012; revised manuscript received Jun. 20, 2012; accepted for publication Jun. 22, 2012; published online Jul. 25, 2012.

1 Introduction

The two major forms of inflammatory bowel diseases (IBD), Crohn's disease (CD) and ulcerative colitis (UC), are chronic remittent inflammations that may affect the entire gastrointestinal tract. IBD usually requires life-long treatment and affects mainly young people. Long-term studies have revealed a general increase in the prevalence of both diseases in Europe, Northern America, and Asiatic countries.[1] Both types of IBD occur in genetically susceptible individuals through interplay with poorly understood environmental factors.

The intestinal epithelium in IBD acting as an immunophysiologic barrier might represent the sole factor antecedent to the development of IBD. The epithelium can be leaky due to dysfunction of cell–cell adhesion via tight-junctions.[2] Resorptive epithelium cells (enterocytes) can act disordered in antigen-recognition, uptake, and processing.[3] It is established that enterocytes can change their protein profile under conditions of different proinflammatory cytokines like Interferon-γ, IL-1β, and IL-6.[4] In addition, it is known that enterocytes from patients with IBD show distinct differences in protein expression profile.[5]

The distinction between UC and CD is made based on clinical, endoscopic, radiologic, and pathologic features.[6] However, for about 15 to 20% of the patients it is not possible to classify them into either one of the IBD forms, with the result that diagnostics and therapy cannot be given, as requested, to these patients. This demonstrates the unmet medical need for a deeper understanding of IBD pathogenesis as well as for better diagnostic methods.

Raman microspectroscopy has proven in the last years to be a promising method for biomedical cell and tissue diagnostics.[7] Tissue Raman spectra can be correlated with the histopathology of tissue, since the tissue Raman signature reflects its biochemical composition. The potential of Raman microspectroscopy for gastrointestinal diagnostics has been demonstrated recently.[8,9] Furthermore, Raman microscpectroscopy has been applied in gastrointestinal oncology as diagnostic tool to characterize single cancer cells[10] and early malignat changes in tissue sections.[11,12] Also, *in vivo* Raman applications to achieve better diagnostic results for dysplastic diseases have been reported.[13] In contrast, little has been reported about using Raman spectroscopy to detect molecular changes taking place in epithelial cells during inflammatory conditions. A recently published study from Bi et al.[14] demonstrated for the first time the potential of Raman spectroscopy (in particular fiber-optic Raman spectroscopy) in IBD by showing that Raman band heights differ for UC and CD. However, in this preliminary study no control specimens, required in order to establish Raman spectroscopy as diagnostic procedure, were included.

Here, we propose a Raman mapping approach to establish Raman spectroscopy as a diagnostic method for healthy control

*Authors contributed equally to this work.

Address all correspondence to: A. Stallmach, Department of Internal Medicine II, Division of Gastroenterology, Hepatology, and Infectious Diseases, University Hospital Jena, Jena, Germany; E-mail: andreas.stallmach@med.uni-jena.de; J. Popp, Institute of Physical Chemistry and Abbe Center of Photonics, Friedrich-Schiller-University, Jena, Germany; Institute of Photonic Technology, Albert Einstein Straße 9, Jena, Germany; E-mail: juergen.popp@uni-jena.de

0091-3286/2012/$25.00 © 2012 SPIE

patients (HC), patients with CD, and patients with UC. Since enterocytes are mainly involved in IBD pathogenesis, a classification model was trained to identify/visualize the tissue morphology and to separate the epithelium of IBD and control patients from other tissue species. Afterward the epithelium Raman spectra can be used to classify HC, CD, and UC.

2 Materials and Methods

2.1 *Tissue Preparation*

Colon tissue samples (biopsy) were obtained from the Endoscopic Department, Clinic for Internal Medicine II, Department of Gastroenterology, University Medical Center in Jena, Germany. Before the colonoscopy, patients gave informed consent for the study procedure prior to colonoscopy. Samples were taken from healthy control patients ($n = 11$) undergoing a colonoscopy for surveillance purposes and from patients with IBD ($n = 27$). In total, 14 patients with CD and 13 patients with UC were included. Biopsies were taken from endoscopic normal or moderately inflammed areas. The local ethics commission approved the study protocol.

For each specimen, fresh samples were taken and immediately frozen in liquid nitrogen. Samples were stored at −80°C. On the day of the Raman measurements, tissue cryosections, 10 μm thick, were attached to calcium fluoride slides (CaF_2). Consecutive sections were cut from each sample, placed on a microscope glass slide, and stained with hematoxylin and eosin (H&E) for histopathological examination to define the Raman measurement region. The protocol for the H&E staining was as follows: fixation [methanol ($1 \times 3'$) and acetone ($1 \times 3'$)], rinsing ($1 \times 2'$ deionized water), the Hematoxylin staining {$1 \times 5'$ [Mayer's hemalum solution (Sigma Aldrich)]}, rinsing ($1 \times 10'$ tap water, deionized water $1 \times 1'$), the eosin staining {$1 \times 5'$ [eosin Y solution 0.5% aqueous (Merck)]} and a dehydration (ethanol 80%, 98%, and 100% $1 \times 1'$). After this a xylene-fixation was carried out. The Raman measurement region was chosen in such a way that an epithelium layer consisting of 5 to 8 epithelial cells was located in the measured area. Subsequent to the Raman measurement, the tissue sections on the CaF_2 slide were H&E stained and imaged (Zeiss-Axioplan 2 imaging HBO 100, objective: $40 \times /0.75$ Plan-Neofluar) to reassess the Raman scanned area.

2.2 *Raman Instrumentation*

Raman spectra were recorded with a Raman microspectrometer (Kaiser Optical Systems, Ann Arbor, MI) using a diode laser at 785 nm as excitation wavelength. The laser light was focused on the sample with a $100 \times$/NA 0.9 objective (Nikon, Japan) to give ≈200 mW on the sample. The scattered Raman signal was detected on a Peltier-cooled, back-illuminated, deep-depletion CCD chip (Andor, Northern Ireland) after passing a holographic transmissive grating. Raman scans were acquired in the mapping mode using a motorized xy-sample stage with step-size 1.5 μm. The exposure time for each spectrum was 5 s, and an additional dwell time of 10 s was necessary to reduce the autofluorescence of the tissue. Cosmic ray removal and intensity correction were automatically performed by the Kaiser HoloSpec software.

2.3 *Chemometrics*

The Raman spectra were subjected to a multivariate data analysis and the results were correlated with the histomorphology of the tissue. All of the computations were done using gnu R[15] running on a commercial available PC system (Intel(R) Core(TM) 2Duo CPU, E6750 2.66 GHz, 1.97 GB RAM).

Prior to the chemometric analysis, the Raman spectra must be preprocessed to correct for corrupting signals due to the experimental setup and the sample itself.[16] This Raman data preprocessing procedure is briefly summarized as follows. First, a wavenumber calibration has been performed using the 322 cm^{-1} band of CaF_2, followed by truncating the wavenumber region to 250 to 3100 cm^{-1} and background removal applying a SNIP algorithm.[17] Thereafter the spectral range was further narrowed to 675 to 3020 cm^{-1} and the wavenumber areas 944 to 996 cm^{-1} and 1725 to 2815 cm^{-1} were excluded due to artefacts and no Raman signals occurring in these regions, respectively. At the end of this preprocessing procedure a vector normalization was performed followed by a principal component analysis (PCA)[18,19] using only the first 50 PCs.

For the chemometric analysis, a k-means-cluster-analysis (KM)[20,21] and support-vector-machines (SVM)[22,23] were applied. In the following a brief description of both methods is given. KM is an unsupervised algorithm, which aims to group the dataset into a given number of groups (cluster). It starts with a random distribution, and calculates the means of the groups and the distance of all Raman spectra to the means. After resorting, every spectrum is placed in its nearest cluster, the means are updated, and this is done until a stable arrangement is reached. Every cluster is color-coded and the spatial arrangement of these clusters is displayed in a false-color-plot. SVM is a classification technique used to build up a model based on group differences. This method searches for the hyperplane, which separates two groups in the best way. Here the radial-base kernel is utilized and the SVMs for multiclass tasks are combined by the one-against-one scheme. At the end the performance of the SVM is evaluated by a 10-fold cross-validation[24] in order to check the prediction ability of the model.

The dataset of the present study consist of total 38 scans with 80,356 Raman spectra containing 13 scans emanated from donors with UC (30,008 Raman spectra), 14 scans from patients with CD (26051 Raman spectra), and 11 scans from healthy control patients (25,279 Raman spectra). The dimension of the scans ranges from 46.5×40.5 μm^2 to 135×60 μm^2.

3 Results and Discussion

Raman imaging was performed for 38 biopsy samples, and for all of these biopsy samples it was possible to highlight the colonic mucosa together with epithelium cells. In order to differentiate between the different tissue components, a complex Raman analysis strategy was carried out to visualize the epithelium and to classify healthy control patients, patients with CD, and patients with UC. The workflow of this Raman analysis procedure is displayed in Fig. 1 and summarized in the following.

Every Raman scan was preprocessed as described above followed by a k-means-cluster-analysis with $k = 10$ leading to a false-color-plot (upper left corner of Fig. 1), which can be compared with the corresponding H&E image of the same area (upper row, middle image in Fig. 1). By doing so, an experienced pathologist can assign every Raman cluster to one of five groups (upper right corner of Fig. 1): while epithelium (E),

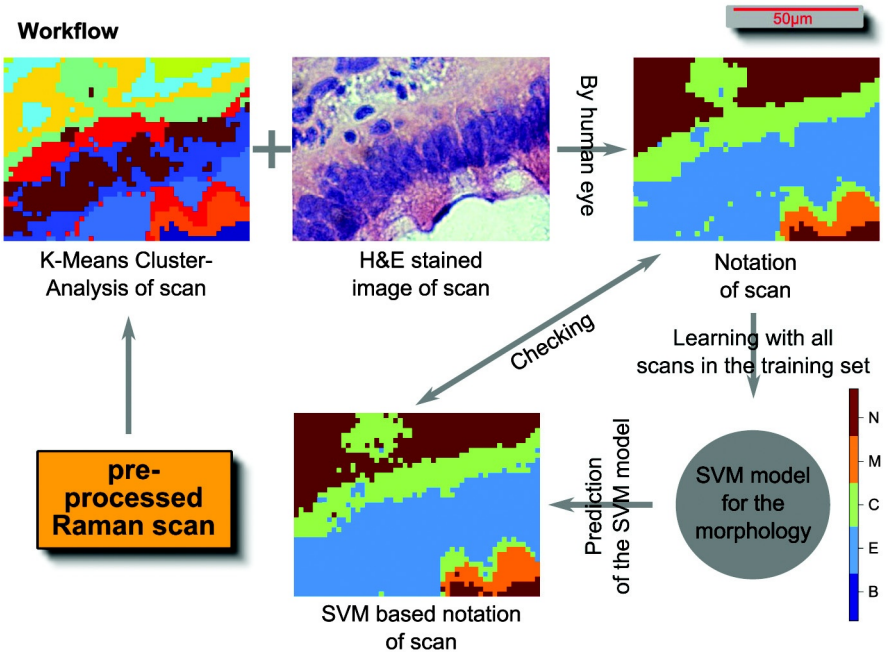

Fig. 1 Workflow of the analysis: After the spectral preprocessing a *k*-means-cluster-analysis is carried out and every cluster is allocated to a morphological feature (blood B, epithelium E, connective tissue C, mucus M, not notable N) by a pathologist. This notation is subsequently learned by a support vector machine (SVM) and the prediction quality is estimated using a 10-fold cross-validation with the notation of the pathologist as reference. Every SVM prediction is additionally compared with the corresponding H&E-stained image, which indicates that the SVM prediction can be seen as spectral histopathology, i.e., a computational H&E stain.

mucus (M), connective tissue (C), and blood (B) represent a common histopathologic rating, the last group (not notable, N) is of particular relevance for training the classification algorithm. Subsequent to this *k*-means-cluster-analysis, a SVM was used for learning these five groups, which represent the tissue morphology. The resulting SVM model is capable of visualizing the five groups and especially the epithelium region (cyan). The quality of this SVM assignment can be evaluated by comparing the notation of the pathologist with SVM based notation (lower right corner of Fig. 1). In addition to this first classification step, a second step was established exclusively utilizing the epithelium Raman spectra for IBD diagnosis. The whole hierarchical classification system was evaluated by a 10-fold cross-validation (CV) and statistical properties like sensitivity, selectivity, and correct classification rate, which were estimated by using the cross-validation. It should be noted that the hierarchical classification system was designed in such a way that it can be used as *in vivo* diagnostic method.

3.1 *First Level—Morphology Visualization*

First we checked to determine whether the pathological assignment is reflected by the Raman data. Therefore, the mean Raman spectra [Fig. 2(a)] of the five groups specified above were inspected and differences between these mean Raman spectra were calculated [Fig. 2(b)]. While the mean Raman spectrum of blood is dominated by resonance Raman contributions from hemoglobin,[25] the other four mean Raman spectra are dominated by bands, which can be assigned to proteins, lipids, and nucleic acids to a small extent. Figure 2(b) shows the difference spectra of the C, N, and M groups with the epithelium group (E): the negative bands at 743, 1245, and 1580 cm^{-1} in the N-E and C-E difference spectra can be assigned to heme vibrations.[25] This finding is reasonable because IBDs are chronic inflammatory diseases in which the colonic mucosa often appears with a lot of bleeding signs. The mucus-epithelium difference spectrum shown in Fig. 2(b) is characterized by difference bands at 835, 1041, 1140, 1280, and 1380 cm^{-1}, which arise due to the different composition of mucus (M) as compared to epithelium (E).

In addition to wavenumber positions, we evaluated the band intensities of the following characteristic vibrations: 1003 cm^{-1} (phenylalanine ring breathing), 1450 cm^{-1} (CH_2-deformation), 1305 cm^{-1} (CH_2-twisting), 1245 cm^{-1} (amide III), and 1660 cm^{-1} (amide I and C = C-stretching), which can be used to characterize the protein-lipid composition of biological tissue:[26,27] while the the first band at 1003 cm^{-1} can be used as marker for proteins, the vibrations at 1450 cm^{-1} and 1305 cm^{-1} display biomaterial and lipid content, respectively. The two other bands at 1245 cm^{-1} and 1660 cm^{-1} can be assigned to heme and also to lipids and proteins. These five bands form a so-called metric[28] and are used throughout this paper. This metric was chosen according to Mahadevan-Jansen et al.[29] who discriminated between cervical epithelium, inflammation, metaplasia, low-grade and high grade lesions utilizing Raman bands at 1246, 1330, 1454, and 1656 cm^{-1} that are similar to our metric. After calculating the band heights of these five Raman bands, a (two-sided) Student's *t*-test[30,31] was performed between all combinations of groups (B, E, C, M, N) and for all band heights. The obtained *p*-values were all smaller than 10^{-19} and therefore the significance level was ***. Here the common definition of the significance levels (* $p < 0.05$; ** $p < 0.01$; *** $p < 0.001$) was utilized. This result permits the training of a classification technique.

For classification, a SVM with the PCA scores as input was applied. The resulting morphology classification model can be visualized by the score plot of the decision values [see Fig. 3(a)

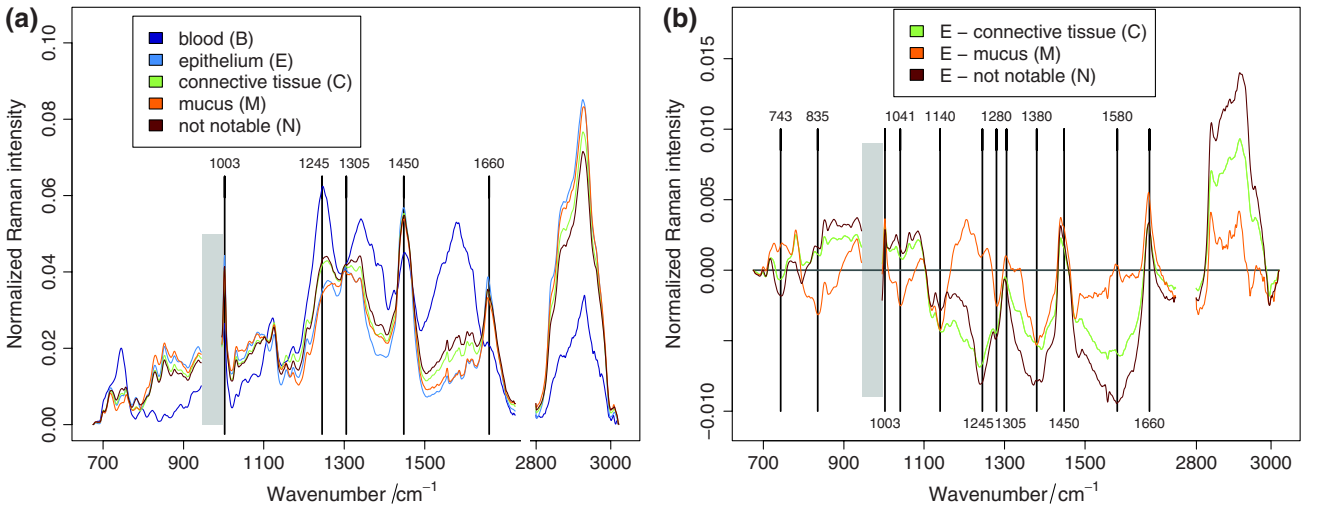

Fig. 2 (a) Mean Raman spectra of the morphological tissue arrangement: The spectral differences between the blood Raman spectrum and the other mean spectra are obvious, which is due to the resonant contribution of hemoglobin. Even though the differences between the E, C, M, and N spectra are smaller, they were proven to be significant by a *t*-test. For details see text. (b) Difference spectra of the mean Raman spectra. The difference of E-C and E-N are dominated by heme-vibrations (743, 1245, and 1580 cm^{-1}), while the bands observed in the difference spectrum E-M (835, 1041, 1140, 1280, and 1380 cm^{-1}) are caused by the different biochemical constitution of mucus.

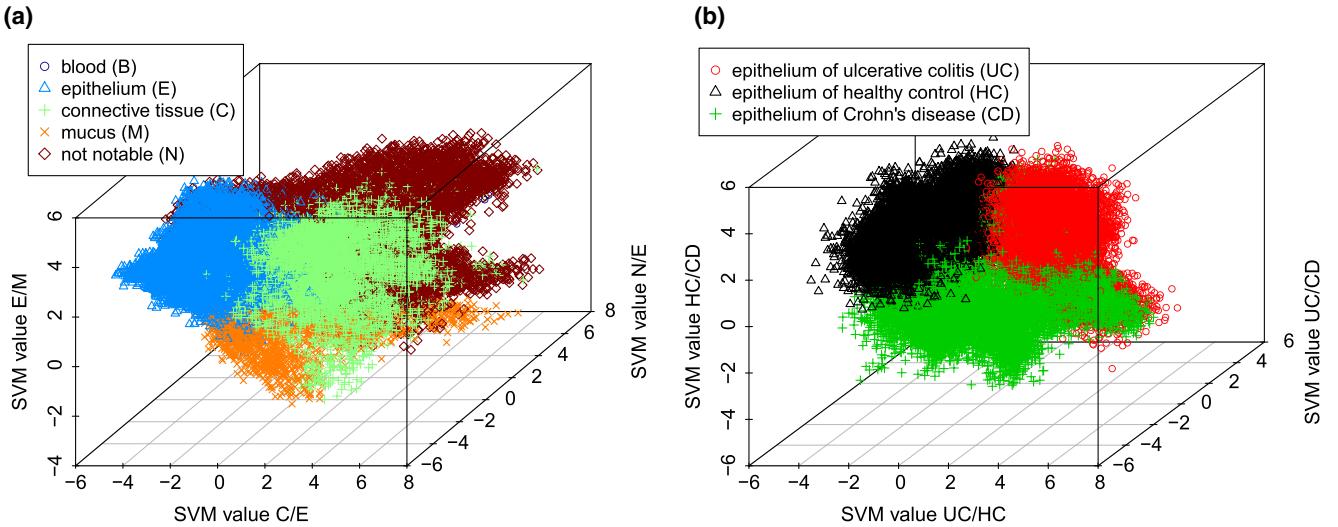

Fig. 3 (a) Decision values of the first level SVM (morphology): The separation of the four groups (E, C, M, N) is obvious. The blood group is not visible because the Raman spectra of that group are hidden by the other Raman spectra. (b) Decision values of the second level classification (disease recognition) are visualized. The three groups HC, CD, and UC show good separated data clouds.

where three out of 10 decision values (C/E, N/E, and E/M) are displayed]. The separation of the clouds in Fig. 3(a) is a clear indicator for a valid model. The prediction ability of the model was evaluated by a 10-fold cross-validation and is shown in Table 1. From this table the correct classification rate can be calculated to be (91.85%). Also the sensitivity, specificity, and selectivity for finding the epithelium (E) were computed, which were 93.84%, 90.30%, and 88.26%, respectively. The relatively low classification rate of only 91.85% is not a crucial problem, because this low value results from the notation procedure, which will be discussed below.

Panels A of Figs. 4 and 5 show two H&E images of colon tissue sections where the area investigated by means of Raman microspectroscopy is marked by a black rectangle. In panels F the results of a *k*-means-cluster-analysis with $k = 10$, which has been further used to generate the notation plot presented in panels E, is shown. It should be noted that the colors used in panels F are chosen arbitrarily, while the colors used in the notation plot (panels E) reflect the morphological features described above (i.e., B = blue, E = cyan, C = green, M = orange, N = brown). Panels D of Figs. 4 and 5 display the SVM-based notation and can be seen as the sample's spectral histopathology. Panels C highlight the wrongly classified pixels that are pixels marked in red where the notation (E) and the SVM notation (D) differ. Most of the misclassifications can be found at the borders between the different regions and where the pathologist was uncertain and assigned it to the N-group. The latter can be found, for example, in Fig. 4 at the top side edge: a cluster [yellow in panel Fig. 4(f)] that was labeled as N by the pathologist has been classified by the SVM to the

Table 1 Confidence table of a SVM, which learned the morphological notation. The classification rate of only 91.85% is no problem, because it was calculated with the notation of the pathologist. It is of much more importance that the morphological features were reproduced correctly compared with the H&E-stained image (see Figs. 4 and 5).

		Prediction				
Color	Notation	B	E	C	M	N
Blue	Blood (B)	21	0	0	0	5
Cyan	Epithelium (E)	0	32970	360	51	1752
Green	Connective tissue (C)	0	1107	5554	36	1216
Orange	Mucus (M)	0	298	109	1326	140
Brown	Not notable (N)	0	2980	393	63	31975

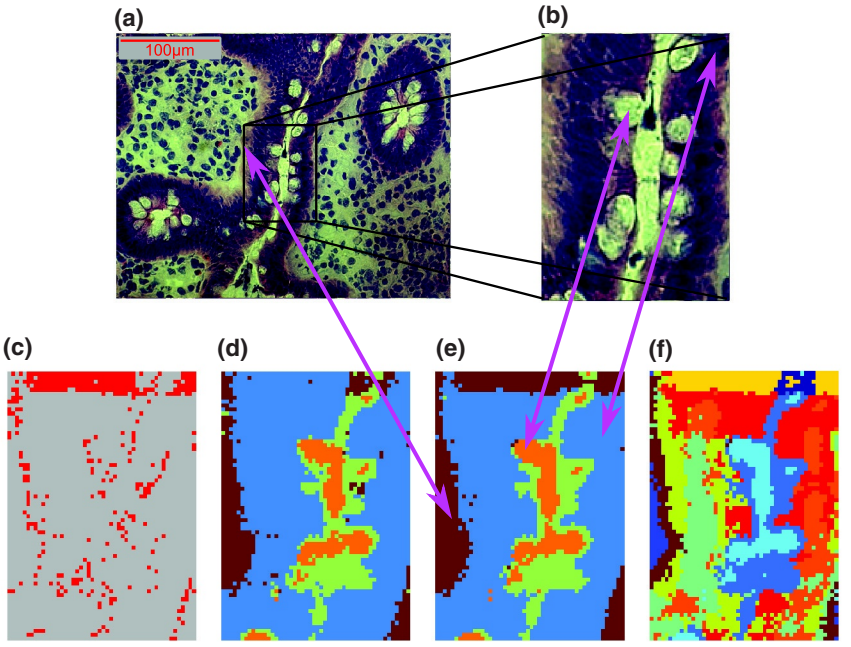

Fig. 4 Results derived from a Raman scan from the UC group (one example out of 13); (a) H&E-stained image where the Raman scanned region is marked by a rectangle; (b) H&E zoomed area investigated by Raman spectroscopy; (f) false-color-plot of a *k*-means-cluster-analysis of the Raman map; (e) (morphological) notation by a pathologist; (d) SVM based notation; (c) difference of both notations. For details see text.

epithelium group [cyan in Fig. 4(d)], which seems to fit better to the H&E image [Fig. 4(b)]. However, these misclassification errors are not a problem as long as the SVM-learned images [Figs. 4(d) and 5(d)] display the same properties as the corresponding H&E images [Figs. 4(b) and 5(b)], which is fulfilled here for all of the 38 scans. For both examples shown in Figs. 4 and 5 the epithelium, connective tissue, and mucosa regions, visible in the H&E images [Figs. 4(b) and 5(b)], are reproduced well in the corresponding SVM-learned images [Figs. 4(e) and 5(e)]. It should be noted that empty goblet cells were assigned to the N-group due to their weak Raman intensity. In contrast goblet cells filled with mucus were grouped as "M" (see Fig. 5).

To summarize, the analysis of Raman maps by chemometric approaches allows one to generate images providing the same information as H&E images ("computational H&E stain"), which is why this approach can be referred to as spectral histopathology, which—in principle—can be applied under *in vivo* conditions. In other words, all features of the H&E images [Figs. 4(b) and 5(b)] can be also found in the SVM-based notation [Figs. 4(e) and 5(e)]. Such a morphological presorting step is necessary, if the epithelium is of diagnostic relevance (as, for instance, in the diagnosis of cancer or IBD). In case such a morphological presorting step is skipped, the observed spectral differences might be caused by different measured areas and not by a different biochemistry of the sample.

3.2 *Second Level—Disease Recognition*

In the previous section it has been shown that it is possible to establish a statistical model for a histopathological classification of Raman maps. In the following section, the Raman spectra of only the epithelium region identified by this approach will be

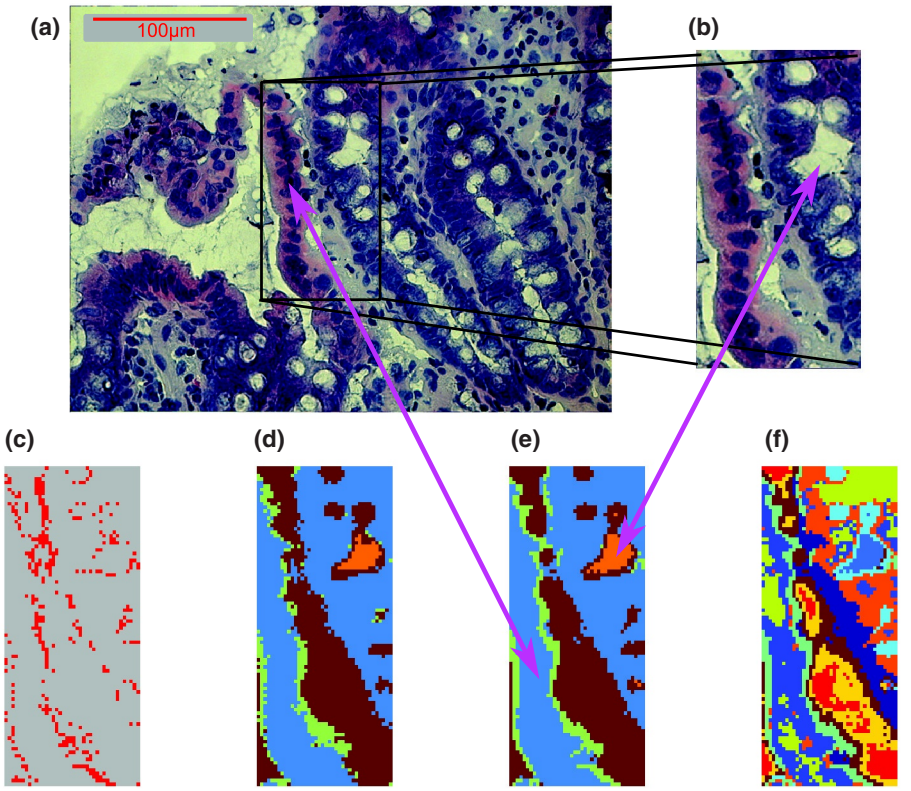

Fig. 5 Results derived from a Raman scan from the control group (one example out of 11); (a) H&E-stained image where the Raman scanned region is marked by a rectangular; B: H&E zoomed area investigated by Raman spectroscopy; (f) false-color-plot of a *k*-means-cluster-analysis of the Raman map; (e) (morphological) notation by a pathologist; (d) SVM-based notation; (c) difference of both notations. For details see text.

used to build up a classification model for the differentiation of HC from IBD. Therefore, as for the morphology classification reported in the previous section, a SVM was applied. By doing so the SVM was trained by the Raman spectra of the epithelium region to achieve a separation between epithelium Raman spectra from healthy control patients, patients with CD, and patients with UC. The corresponding mean Raman spectra of these three groups are plotted in Fig. 6(a). It can be seen that the three Raman spectra are rather similar, characterized by only small subtle spectral differences [see difference plot in Fig. 6(b)]. However, this similarity is not surprising since the epithelium region for HC, CD, and UC are roughly of the same biochemical composition. Nevertheless, the difference spectrum of UC-HC and CD-HC [see Fig. 6(b)] exhibits some differences, mainly at 743, 1245, and 1580 cm^{-1} where prominent Raman bands of heme can be found. The different heme contributions can be

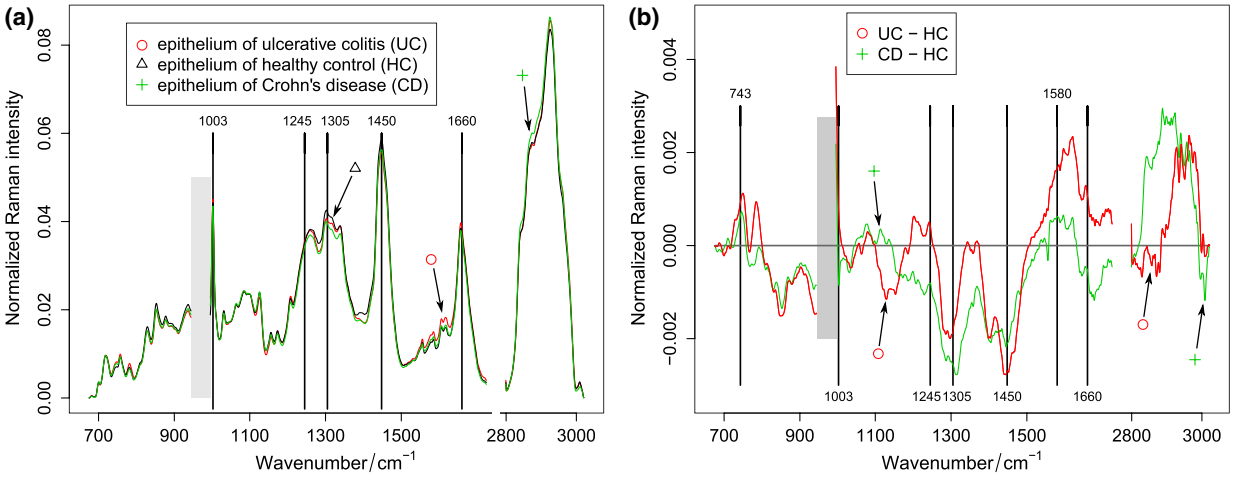

Fig. 6 (a) mean Raman spectra of the epithelium of the three groups (HC, UC, CD). (b) Corresponding difference Raman spectra. The main differences can be assigned to bands of heme (743, 1245, and 1580 cm^{-1}), which can be explained by characteristic hyperemic colonic mucosa in UC in contrast to CD and HC. For details see text.

Table 2 Second-level classification based on epithelium Raman spectra evaluated by 10-fold cross-validation. The correct classification rate was 98.90%, while the sensitivity and specificity for detecting the HC-group are 99.07% and 98.81%.

	Predicted		
True	UC	HC	CD
Ulcerative colitis (UC)	12675	59	65
Healthy control (HC)	27	13109	96
Crohn's disease (CD)	85	78	11168

explained by the inflammation of the colonic mucosa in patients with IBD as compared to HC and by a characteristic hyperemic colonic mucosa in UC in contrast to CD. Beside these major spectral differences, some minor differences for protein and lipid Raman bands also exist. Now the question arises of whether these spectral differences in the epithelium Raman spectra of the three classes HC, CD and UC are significant and enable a reliable IBD diagnosis. This question will be pursued in the following.

To start with, a *t*-test[30,31] was carried out, in order to check if these subtle spectral differences are significant. In doing, so the band heights of the metric defined above (i.e., of the Raman bands at 1003, 1450, 1305, 1245 and 1660 cm^{-1}) were calculated. For all *p*-values of every band and for every combination of groups (UC, CD, HC), significance level *** was obtained, clearly demonstrating that the spectral differences are significant. This finding agrees with the results of Bi et al.[14] However, the significance level of $p < 0.001$ (***) found here is better than the one of $p < 0.05$ (*) found by Bi et al.[14] Furthermore, we identified a significant difference between IBD and HC, which is a key feature for establishing an IBD diagnostic procedure.

After the significance was proven, a classification model (SVM) was trained using the PCA scores of the epithelium Raman spectra as input. The prediction quality of the model was evaluated by a 10-fold cross-validation. The results are summarized in a confidence table (Table 2), clearly demonstrating that the three groups (HC, UC, and CD) are well separable, resulting in a very good classification rate of 98.90%. The sensitivity and specificity for detecting the HC-group are with 99.07% and 98.81%, also very high. Overall, the performance of the trained SVM model is extremely good, showing that the spectral differences between the epithelium Raman spectra of HC, UC, and CD are significant. These spectral differences point toward different chemical compositions of HC, UC, and CD, e.g., different protein patterns of epithelium cells in HC, UC, and CD. This finding is additionally confirmed by the decision value plot of the SVM [Fig. 3(b)], where the three groups form well-separated clusters. To sum up it can be said that the presented results can be seen as a first promising step toward a Raman spectroscopy–based IBD diagnostic method.

4 Conclusion

The results presented in this study show that Raman spectroscopy can be used to diagnose IBDs. In detail 38 Raman maps of colon tissue sections of patients with CD, patients with UC, and healthy control patients were generated. The resulting Raman maps were subjected to *k*-means clustering, and the generated cluster maps were morphologically analyzed by a pathologist. This morphological notation was subsequently learned by a SVM, allowing for an automatic calculation of the morphology. This step can be seen as spectral histopathology or "computational H&E staining," since the same morphological information can be extracted from the SVM-generated image as compared to a classical H&E picture but without staining. This first-level SVM analysis was afterward used to differentiate the epithelium Raman spectra (E) from the Raman spectra of connective tissue (C), blood (B), mucus (M), and other Raman spectra (N). This presorting step is crucial for diagnosing diseases affecting the mucosal epithelium in particular for dysplasia (e.g., colonic cancer) or inflammation (e.g., IBD) of the colonic mucosa.

In a second step, the epithelium Raman spectra were further investigated in terms of proving if the Raman spectral signatures of the epithelium of healthy control patients and those of patients with IBD are different. An analysis of the epithelium Raman spectra showed that the epithelium regions of HC and IBD are characterized by a significantly different epithelium biochemistry. Moreover, it was also found that the epithelium Raman spectra of CD and UC exhibit pronounced spectral differences. These spectral differences allow for discriminating between UC and CD based on epithelium Raman spectra. The resulting SVM classifier yielded a classification rate of 98.90%.

Overall we were able to show for the first time that Raman imaging allows for a differentiation between healthy control patients, patients with CD, and patients with UC. The established classification model can be used in further studies to diagnose patients with unclassified IBD (colitis indeterminata), which is still a big challenge in IBD treatment. Furthermore, a classification model taking into account a larger dataset might be even able to distinguish between different inflammation stages of IBD. Furthermore, it should be mentioned that the herein presented hierarchical classification approach is fully automatic and can therefore be used under *in vivo* conditions (i.e., for nondried specimens), showing that Raman-based IBD diagnosis is possible.

Acknowledgments

Financial support of the European Union via the Europäischer Fonds für Regionale Entwicklung (EFRE), the financial support of the 'Thüringer Ministerium für Bildung, Wissenschaft und Kultur' (project JenZIG: B714-07037), the funding of the research projects BI 1490/1-1, PO 563/13-1 and STA 295/9-1 from the German Research Foundation (DFG) and the financial support from the Interdisciplinary Center for Clinical Research (IZKF) of the University Medical Center Jena are gratefully acknowledged.

References

1. V. Binder, "Epidemiology of IBD during the twentieth century: an integrated view," *Best Pract. Res. Clin. Gastroenterol.* **18**(3), 463–479 (2004).
2. J. Söderholm et al., "Augmented increase in tight junction permeability by luminal stimuli in the non-inflamed ileum of Crohn's disease," *Gut* **50**(3), 307–313 (2002).
3. G. Hundorfean et al., "Luminal antigens access late endosomes of intestinal epithelial cells enriched in MHC i and MHC ii molecules: in vivo study in Crohn's ileitis," *Am. J. Physiol. Gastrointest. Liver Physiol.* **293**(4), G798–G808 (2007).

4. S. Barceló-Batllori et al., "Proteomic analysis of cytokine induced proteins in human intestinal epithelial cells: implications for inflammatory bowel diseases," *Proteomics* **2**(5), 551–560 (2002).
5. A. Shkoda et al., "Differential protein expression profile in the intestinal epithelium from patients with inflammatory bowel disease," *J. Proteome Res.* **6**(3), 1114–1125 (2007).
6. D. Podolsky, "Inflammatory bowel disease," *N. Engl. J. Med.* **325**(13), 928–937 (1991).
7. C. Krafft, B. Dietzek, and J. Popp, "Raman and CARS microspectroscopy of cells and tissues," *Analyst* **134**(6), 1046–1057 (2009).
8. C. Krafft et al., "Raman and FTIR microscopic imaging of colon tissue: a comparative study," *J. Biophoton.* **1**(2), 154–169 (2008).
9. C. Krafft et al., "A comparative Raman and CARS imaging study of colon tissue," *J. Biophoton.* **2**(5), 303–312 (2009).
10. K. Chen et al., "Diagnosis of colorectal cancer using Raman spectroscopy of laser-trapped single living epithelial cells," *Opt. Lett.* **31**(13), 2015–2017 (2006).
11. A. Beljebbar et al., "Identification of Raman spectroscopic markers for the characterization of normal and adenocarcinomatous colonic tissues," *Crit. Rev. Oncol. Hematol.* **72**(3), 255–264 (2009).
12. E. Widjaja, W. Zheng, and Z. Huang, "Classification of colonic tissues using near-infrared Raman spectroscopy and support vector machines," *Int. J. Oncol.* **32**(3), 653–662 (2008).
13. M. Bergholt et al., "Characterizing variability in in vivo Raman spectra of different anatomical locations in the upper gastrointestinal tract toward cancer detection," *J. Biomed. Opt.* **16**(3), 037003 (2011).
14. X. Bi et al., "Development of spectral markers for the discrimination of ulcerative colitis and crohn's disease using raman spectroscopy," *Dis. Colon Rectum* **54**(1), 48–53 (2011).
15. R Development Core Team, R: A Language and Environment for Statistical Computing, R Foundation for Statistical Computing, Vienna, Austria (2007), http://www.R-project.org.
16. T. Bocklitz et al., "How to pre-process Raman spectra for reliable and stable models?" *Anal. Chim. Acta* **704**(1–2), 47–56 (2011).
17. C. Ryan et al., "SNIP, a statistics-sensitive background treatment for the quantitative analysis of pixe spectra in geosience aplications," *Nucl. Instrum. Meth. B* **34**(3), 396–402 (1988).
18. K. Pearson, "On lines and planes of closest fit to systems of points in space," *Philosophical Magazine* **2**(6), 559–572 (1901).
19. S. Wold, K. Esbensen, and P. Geladi, "Principal component analysis," *Chemometr. Intell. Lab.* **2**(1–3), 37–52 (1987).
20. C. Ding and X. He, "K-means clustering via principal component analysis," in *Proc. of the 21st International Conference on Machine Learning*, Banff, Canada (2004).
21. P. Lasch et al., "Imaging of colorectal adenocarcinoma using ft-ir-microspectroscopy and cluster analysis," *Biochim. Biophys. Acta* **1688**(2), 176–186 (2004).
22. C. J. C. Burges, "A tutorial on support vector machines for pattern recognition," *Data. Min. Knowl. Disc.* **2**(2), 121–167 (1998).
23. T. Hastie, R. Tibshirani, and J. Friedman, *The Elements of Statistical Learning—Data Mining, Inference, and Prediction*, Springer, New York (2008).
24. R. Kohavi, "A study of cross-validation and bootstrap for accuracy estimation and model selection," in *Proc. of the International Joint Conference on Artificial Intelligence*, pp. 1137–1143, Morgan Kaufmann, Palo Alto (1995).
25. B. Wood et al., "Resonance Raman spectroscopy of red blood cells using near-infrared laser excitation," *Anal. Bioanal. Chem.* **387**(5), 1691–1703 (2007).
26. C. Krafft et al., "Mapping of single cells by near infrared Raman microspectroscopy," *Vib. Spectrosc.* **32**(1), 75–83 (2003).
27. I. Notingher and L. Hench, "Raman microspectroscopy: a noninvasive tool for studies of individual living cells in vitro," *Expert Rev. Med. Dev.* **3**(2), 215–234 (2006).
28. R. Bhargava, "Towards a practical Fourier transform infrared chemical imaging protocol for cancer histopathology," *Anal. Bioanal. Chem.* **389**(4), 1155–1169 (2007).
29. A. Mahadevan-Jansen et al., "Near-infrared Raman spectroscopy for in vitro detection of cervical precancers," *Photochem. Photobiol.* **68**(1), 123–132 (1998).
30. Student, "The probable error of a mean," *Biometrika* **6**(1), 1–25 (1908).
31. W. N. Venables and B. D. Ripley, *Modern Applied Statistics with S*, 4th ed., Springer, New York (2002).